Environmental Pollution 297 (2022) 118826

Contents lists available at ScienceDirect

Environmental Pollution

journal homepage: www.elsevier.com/locate/envpol

Combining Himawari-8 AOD and deep forest model to obtain city-level distribution of $PM_{2.5}$ in China☆

Zhihao Song [a,b], Bin Chen [a,b,*], Jianping Huang [a,b]

[a] Key Laboratory for Semi-Arid Climate Change of the Ministry of Education, College of Atmospheric Sciences, Lanzhou University, Lanzhou, 730000, China
[b] Collaborative Innovation Center for Western Ecological Safety, Lanzhou, 730000, China

ARTICLE INFO

Keywords:
$PM_{2.5}$
AOD
Himawari-8
Wind field
Machine learning

ABSTRACT

$PM_{2.5}$ (fine particulate matter with aerodynamics diameter <2.5 μm) is the most important component of air pollutants, and has a significant impact on the atmospheric environment and human health. Using satellite remote sensing aerosol optical depth (AOD) to explore the hourly ground $PM_{2.5}$ distribution is very helpful for $PM_{2.5}$ pollution control. In this study, Himawari-8 AOD, meteorological factors, geographic information, and a new deep forest model were used to construct an AOD-$PM_{2.5}$ estimation model in China. Hourly cross-validation results indicated that estimated $PM_{2.5}$ values were consistent with the site observation values, with an R^2 range of 0.82–0.91 and root mean square error (RMSE) of 8.79–14.72 μg/m^3, among which the model performance reached the optimum value between 13:00 and 15:00 Beijing time ($R^2 > 0.9$). Analysis of the correlation coefficient between important features and $PM_{2.5}$ showed that the model performance was related to AOD and affected by meteorological factors, particularly the boundary layer height. Deep forest can detect diurnal variations in pollutant concentrations, which were higher in the morning, peaked at 10:00–11:00, and then began to decline. High-resolution $PM_{2.5}$ concentrations derived from the deep forest model revealed that some cities in China are seriously polluted, such as Xi 'an, Wuhan, and Chengdu. Our model can also capture the direction of $PM_{2.5}$, which conforms to the wind field. The results indicated that due to the combined effect of wind and mountains, some areas in China experience $PM_{2.5}$ pollution accumulation during spring and winter. We need to be vigilant because these areas with high $PM_{2.5}$ concentrations typically occur near cities.

1. Introduction

In the past two decades, China has experienced rapid economic development. However, due to natural changes and human activities, China has gradually become one of the countries with severe $PM_{2.5}$ pollution (Sun et al., 2016; Zhang et al., 2017; Liu et al., 2019b; Li et al., 2021). As a staple air pollutant, $PM_{2.5}$ poses a huge challenge to China's environmental protection authorities in controlling air pollution (Cheng et al., 2013; Zhao et al., 2013; Andersson et al., 2015; Gao et al., 2016; Budnik et al., 2019). Studies have shown that high $PM_{2.5}$ concentrations are more likely to cause haze weather (Huang et al., 2012b; Ji et al., 2012) and impact visibility (Fu et al., 2008; Xiao et al., 2011), while long-term exposure under $PM_{2.5}$ will seriously threaten human life (Huang et al., 2012a; Dimitriou et al., 2013; Xu et al., 2013). $PM_{2.5}$, which contains harmful substances (Kassomenos et al., 2014; Zhang et al., 2019a), can enter the human body through respiration, leading to cardiovascular disease (Cohen et al., 2017), respiratory disease (Guarnieri and Balmes, 2014), and even lung cancer (Liu et al., 2016). To deal with pernicious $PM_{2.5}$, various countries worldwide have carried out extensive monitoring. Since 2013, China has successively established more than 2000 environmental monitoring stations, which can provide real-time $PM_{2.5}$. These observation results also provide validation data sets for many studies on $PM_{2.5}$ concentration estimation studies.

Many studies have shown that there is a strong correlation between AOD and $PM_{2.5}$ (Guo et al., 2009; Xu et al., 2021), and a statistical relationship between them can be constructed (Ma et al., 2016; Yang et al., 2019). By combining satellite remote sensing AOD with ground observation $PM_{2.5}$ and using statistical methods, $PM_{2.5}$ with high spatial coverage can be obtained (Xiao et al., 2017). Hence, a series of $PM_{2.5}$ estimation methods based on satellite remote sensing AOD have

☆ This paper has been recommended for acceptance by Pavlos Kassomenos.

* Corresponding author. Key Laboratory for Semi-Arid Climate Change of the Ministry of Education, College of Atmospheric Sciences, Lanzhou University, Lanzhou, 730000, China.
E-mail address: chenbin@lzu.edu.cn (B. Chen).

https://doi.org/10.1016/j.envpol.2022.118826
Received 1 October 2021; Received in revised form 3 January 2022; Accepted 7 January 2022
Available online 8 January 2022

emerged (Zhang et al., 2021). In earlier studies, Hu et al. (2014) applied multi-angle implementation of atmospheric correction (MAIAC) AOD to estimate $PM_{2.5}$ concentration in the southeastern United States with a linear mixed effects model, and the results reflected the seasonal $PM_{2.5}$ in this region (coefficient of determination, $R^2 = 0.67$). Subsequently, Ma et al. (2014) used the moderate-resolution imaging spectroradiometer (MODIS) AOD and a geographically weighted regression model to estimate $PM_{2.5}$ in China ($R^2 = 0.64$), and the results showed that the serious $PM_{2.5}$ concentration was in the North China Plain, Tarim Basin, and Sichuan Basin.

Although the linear regression AOD–$PM_{2.5}$ model can reflect the variation in $PM_{2.5}$, its accuracy needs to be further improved. Meanwhile, advanced mathematical statistical methods represented by random forest (RF) and neural networks have been used to estimate $PM_{2.5}$ (Hu et al., 2017). Stafoggia et al. (2019) estimated $PM_{2.5}$ in Italy ($R^2 = 0.86$) using MAIAC AOD and meteorological factors based on RF, and the results showed that the Po River Plain area was seriously polluted during 2013–2015. Wei et al. (2019) used MAIAC AOD and RF to bulid an AOD–$PM_{2.5}$ model in China, and the cross-validation R^2 and root mean square error (RMSE) were 0.85 and 15.57 $\mu g/m^3$, respectively. The AOD–$PM_{2.5}$ model based on neural networks also exhibited good performance. Wang and Sun (2019) used AOD, meteorological factors, and gaseous pollutants as input factors to construct a $PM_{2.5}$ estimation model for the Beijing–Tianjin–Hebei region through deep neural networks, and $R^2 = 0.87$ and RMSE = 27.11 $\mu g/m^3$. Li et al. (2017b) established an AOD–$PM_{2.5}$ model suitable for China using a neural network with an R^2 of 0.88, and the model has excellent performance and is significant for the prevention and control of air pollution. However, "black box" neural networks (Ul-Saufie et al., 2013) are insufficient for exploring the feature contribution.

$PM_{2.5}$ concentration has temporal and spatial variations (Zhang et al., 2020a). $PM_{2.5}$ with high temporal and spatial resolution, is required, which is typically not met by polar orbiting satellites, and geostationary meteorological satellites have been gradually applied to estimate $PM_{2.5}$ (Zhang et al., 2019b). Himawari-8 is a geostationary meteorological satellite that is active in the Asia-Pacific region, equipped with a high-resolution advanced Himawari imager (AHI) (Wu et al., 2020). Based on Himawari-8 AOD data, many studies have established a good hourly AOD–$PM_{2.5}$ model in China with an R^2 of 0.81–0.85 (Chen et al., 2019; Song et al., 2021; Xiong et al., 2021). These AOD–$PM_{2.5}$ models can provide the spatial distribution of hourly $PM_{2.5}$ and help to continuously monitor pollutant evolution.

Based on the above research, we introduced a deep forest (DF) machine-learning model, which has a nonlinear structure similar to a neural network and can provide feature importance. The DF avoids the low interpretability of neural networks (Yan et al., 2021), and combines the tree model to increase the model depth. In this study, we designed a multi-layer DF model, combined with the input Himawari-8 AOD, meteorological factors, and geographic information to generate hourly $PM_{2.5}$ with a spatial resolution of 5 km over China in 2018. Furthermore, the study analyzed the $PM_{2.5}$ distribution at the city level and the wind field impact on pollutants.

2. Datasets and methods introduction

2.1. Datasets

2.1.1. Ground $PM_{2.5}$ observations and Himawari-8 AOD

The China Environmental Monitoring Center (CEMC) provides hourly ground $PM_{2.5}$ data, which are calibrated and controlled according to the National Ambient air quality standards GB 3095–2012 (China, 2012) formulated by the Ministry of Ecology and Environment of the People's Republic of China in 2012. During the study period, there were 1605 total environmental monitoring stations. The study period was from January 1, 2018 to December 31, 2018, and the daily data retrieval time was 09:00–16:00 Beijing time (01:00–8:00 UTC). Six regions were used to analyze the regional differences of the AOD–$PM_{2.5}$ model, including Guanzhong Plain (GZP), Beijing–Tianjin–Hebei region (BTH), Sichuan Basin (SCB), Yangtze River Delta region (YRD), Pearl River Delta region (PRD), and Central China (CC), as shown in Figure S1.

Himawari-8 was launched in 2014 and officially began providing data in 2015. Its onboard AHI observes the Earth every 10 min to provide detailed aerosol information in the Asia-Pacific region (Yoshida et al., 2018). In this study, we used Himawari-8 L3 with 500 nm AOD per hour and a spatial resolution of 5 km. Yang et al. (2020) compared Himawari-8 AOD with AERONET (Aerosol Robotic Network) AOD (R^2 of 0.72), but the Himawari-8 AOD value was slightly lower (Gao et al., 2021). As shown in Figure S1, due to the observation range and bright surface, effective data cannot be obtained in Xinjiang, Tibet, and western Sichuan in China.

2.1.2. Meteorological factors and geographic information

The construction of the AOD–$PM_{2.5}$ model should consider meteorological factors and geographical information, which can affect the formation and aggregation of pollutants (Liu et al., 2019a; Pan et al., 2019; Chen et al., 2020; Chen et al., 2021c; Ma et al., 2021) and alter the correlation between AOD and $PM_{2.5}$ (Pinto et al., 2004; Duvall et al., 2012; Guo et al., 2017). Meteorological factors were obtained from ERA5 reanalysis data derived from the European Centre for Medium-Range Weather Forecasts (ECMWF), including boundary layer height (BLH), 2-m temperature (TM), relative humidity (RH), 10-m U and V wind components (U_{10} and V_{10}), surface pressure (SP), and total precipitation (RAIN). The ERA5 datasets had an hourly temporal resolution and a spatial resolution of $0.25^\circ \times 0.25^\circ$ or $0.1^\circ \times 0.1^\circ$ (as table S1 showed). Land cover types were represented by high and low vegetation indices (LH and LL) from ERA5. The ground elevation data (HEIGHT) was SRTM-3 data jointly measured by the National Aeronautics and Space Administration (NASA) and National Imagery and Mapping Agency (NIMA) of the Department of Defense, with a spatial resolution of 90 m. The population density (PD) was derived from the 2015 United Nations adjusted PD data provided by NASA's Socioeconomic Data and Applications Center (SEDAC), with a spatial resolution of approximately $0.04^\circ \times 0.04^\circ$.

2.2. Methods

2.2.1. Data matching

First, the spatial resolution of meteorological factors and geographic information was adjusted to $0.05^\circ \times 0.05^\circ$ (Himawari-8 AOD data grid resolution) by bilinear interpolation. The range of longitude and latitude is 80°E−136°E, 16°N–54°N, and the number of grids is 1121*761 = 853081. Second, based on a grid of $0.05^\circ \times 0.05^\circ$, the hourly $PM_{2.5}$ recorded by environmental monitoring stations in China (80°E−136°E, 16°N–54°N) were matched with AOD data. If there is one station in a grid, the observed value of the station is the corresponding grid value. If there were two or more stations in a grid, the average $PM_{2.5}$ at these stations is the corresponding grid value.

There were 307,502 samples after data matching, of which the sample sizes were 114,331, 43,752, 86,997, and 62,422 in spring (March, April and May), summer (June, July and August), autumn (September, October and November), and winter (December, January and February), respectively. In summer, many clouds affect satellite observations, resulting in a small sample size.

2.2.2. Deep forest

Deep Forest is a novel machine-learning model proposed by Zhou and Feng (2017). The DF replaces the neurons in the neural network with ensemble learners, and one-way propagation between forest layers (hidden layer) means that the next layer receives the output results of the previous layer and continues to transmit to the next layer. A light gradient boosting machine (LightGBM) was added after the forest layer (Zeng et al., 2021) to process the output information of the last forest

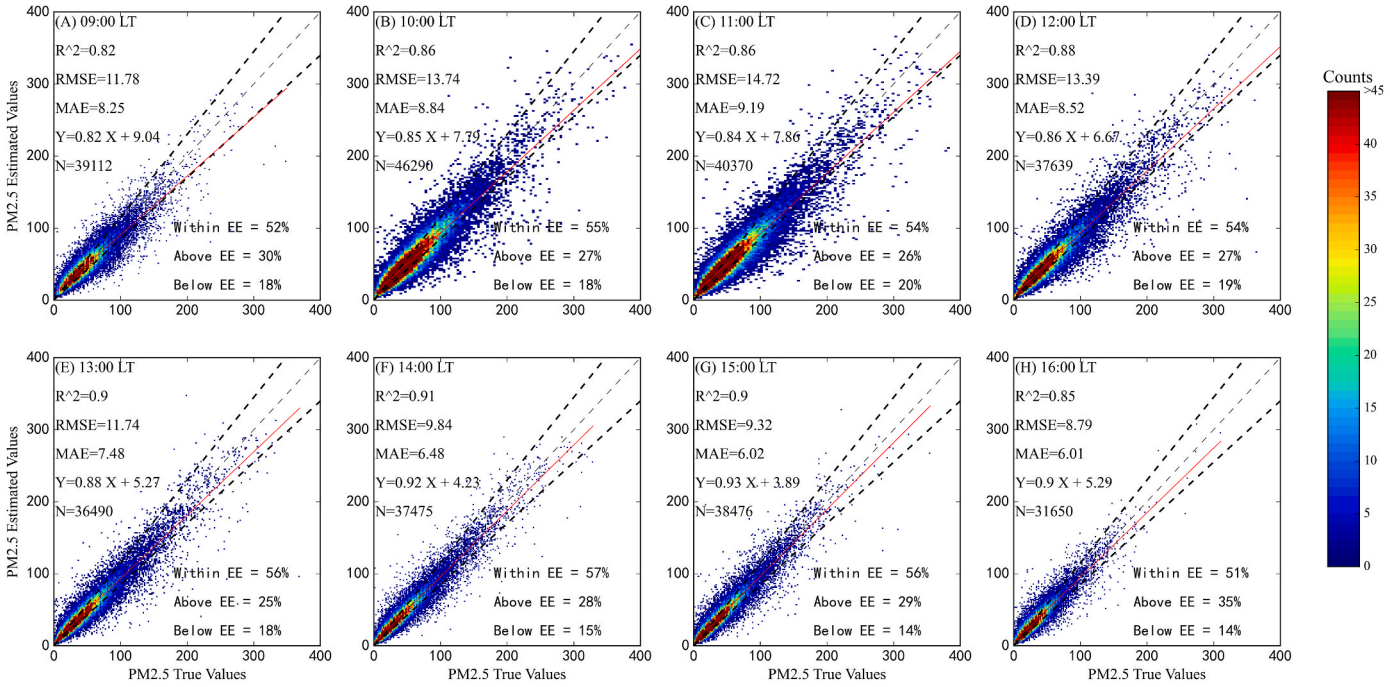

Fig. 1. Hourly model cross-validation results based on sample (the dark dotted line represents the expected error lines, the light dashed line represents the 1:1 line, and the solid red line represents the linear regression fitting line; N indicates the sample size obtained per hour; EE presents the expected error; when the ratio of the estimated value to the true value is between 1.15 and 0.85, the error between them is the expected error(Chu et al., 2002; Yang et al., 2020).). (For interpretation of the references to color in this figure legend, the reader is referred to the Web version of this article.)

layer. Ensemble learners in DFs, including extreme trees (ET) (Chen et al., 2021) and RF (Song et al., 2021), enable the DF to output feature importance (Chen et al., 2022) to help improve the model interpretability. As a deep learning model, the advantage of DF is that it can obtain the importance of model features. For DF model, the parameters to be optimized mainly include the number of forest layers, the number of base learners and the number of decision trees in the base learners. In this study, an AOD–$PM_{2.5}$ DF model with three hidden forest layers was developed, and each layer contained 12 ensemble learners (six ETs and six RFs), and each base learner contains 600 decision trees. The workflow and the structure of the DF model were shown in Figure S2.

The AOD–PM2.5 DF model can be expressed as

$$PM_{2.5\ (i,j)} = f(AOD_{i,j} + BLH_{i,j} + RH_{i,j} + TM_{i,j} + LL_{i,j} + LH_{i,j} + SP_{i,j} + RAIN_{i,j} + U_{10i,j} + V_{10i,j} + PD_{i,j} + HEIGHT_{i,j} + LON\_LAT_j + TIME_i) \quad (1)$$

$PM_{2.5\ (i,j)}$ represents the $PM_{2.5}$ concentration observation value of grid point j at time i, and f represents the DF model. The independent variables include AOD (aerosol optical depth), BLH (boundary layer height), RH (relative humidity), TM (2 m temperature), LL (low vegetation indices), LH (high vegetation indices), SP (surface pressure), RAIN (total precipitation), U_{10} (10 m wind U component), V_{10} (10 m wind V component), PD (population density), HEIGHT (altitude), LON_LAT (spatial variables, formulas (2)), and TIME (temporal variables, formulas (3)) (see Table S1 for details).

$$\text{LON\_LAT} = \frac{lon - lat}{lon + lat} \quad (2)$$

$$\text{TIME} = \frac{seconds}{3600} + 8 \quad (3)$$

In Formula (2), lon and lat represent the longitude and latitude of any grid, respectively, and in Formula (3), seconds represents the total number of seconds between the observation time and 00:00 on January 1, 1900. The spatial variable (LON_ LAT) in this study can represent the relative position of a point on the whole grid by using longitude and latitude combination method. Because the time resolution of Himawari-8 data is hourly, a time stamp accurate to hour was used to represent the temporal feature (TIME) (Wei et al., 2021; Chen et al., 2022). The "TIME" used in our study was a combination of time information (including information about year, month, day and hour), which was similar to the time variable in ERA5 data.

We used a ten-fold cross validation to test the model performance (Rodriguez et al., 2010). The indicators used to describe the model performance include coefficient of determination (R^2), root mean square error (RMSE), mean absolute error (MAE). Firstly, the model performance (R^2, MAE, RMSE) of all samples were calculated. Then, the multiple values of model performance (season, region, hour, etc.) were the average values of all samples by season, region, or hour. Equations and definitions of these indicators can be found in the articles (Chen et al., 2021; Song et al., 2021).

3. Model cross validation results

3.1. Temporal scale validation results

The cross-validation results from 09:00 to 16:00 (Beijing time) in 2018 are shown in Fig. 1. The training data was divided into 10 parts, of which nine parts were used for training the model and one for validation, and the process was repeated ten times. The sampled-based (random sampling of all samples) cross-validation R^2 was 0.82–0.91, fitting slope was 0.82–0.93, RMSE was 8.79 μg/m^3–14.72 μg/m^3, and MAE was 6.01 μg/m^3–9.19 μg/m^3, and the hourly $PM_{2.5}$ derived from the DF model was consistent with ground $PM_{2.5}$ observations. Overall, R^2 was above 0.85 for most of the day, while R^2 was higher than 0.9 between 13:00 and 15:00, which indicated that the AOD–$PM_{2.5}$ model based on DF performed well. Due to changes in meteorological conditions and AOD data quality, model performance varies within a day (Ge et al., 2018; Qin et al., 2018; Zang et al., 2019). Meanwhile, we also performed site-based (random sampling of all sites) validation to test the model performance. As shown in Figure S3, the site-based cross--validation R^2 range was 0.75–0.83 and RMSE (MAE) was 11.14

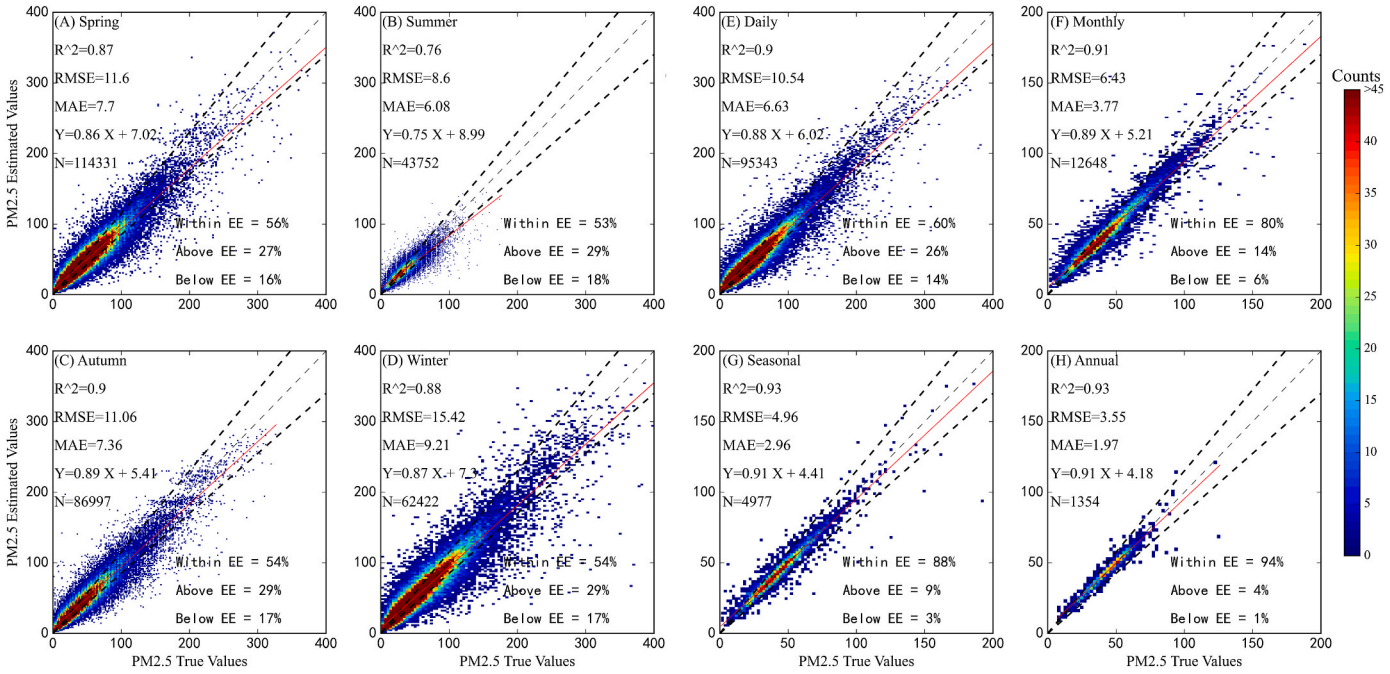

Fig. 2. Same as Fig. 1, but for seasonal and different time scales.

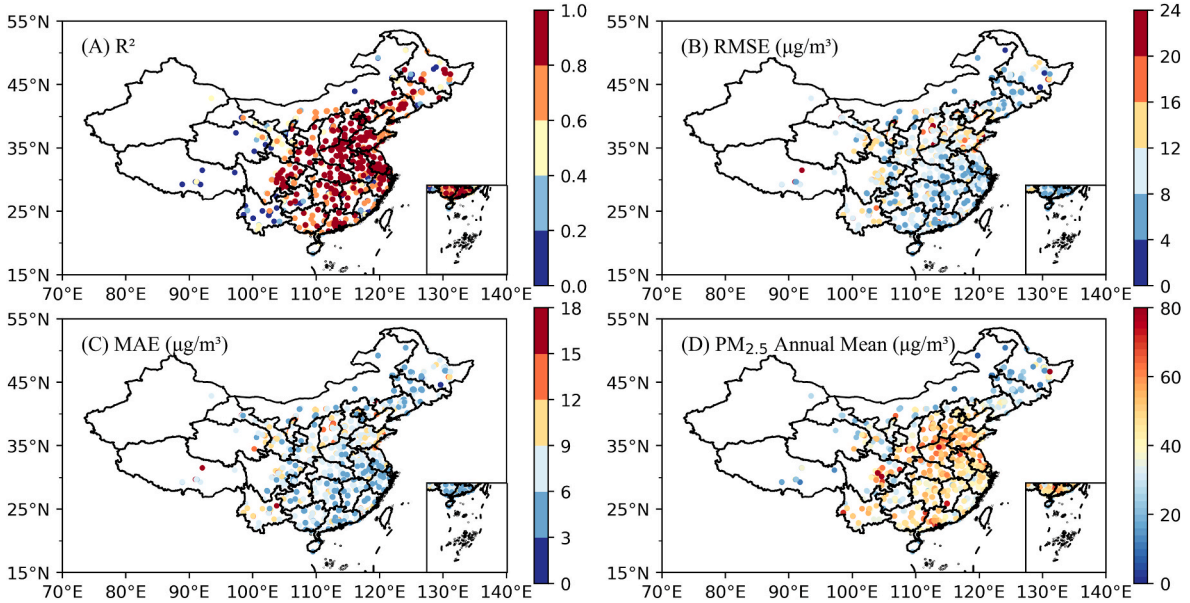

Fig. 3. Spatial distribution of model evaluation indicators (A: R^2, B: RMSE, C: MAE, D: $PM_{2.5}$ annual mean.).

μg/m^3–18.27 μg/m^3 (7.67 μg/m^3–11.46 μg/m^3). The results indicated that the DF model can accurately estimate $PM_{2.5}$ in areas without environmental monitoring stations, but the site-based validation results are lower than the sample-based validation results (Shen and Li, 2019). In addition, The Table S2 shown some results of estimating $PM_{2.5}$ using different machine learning models based on himawari-8 AOD. According to the comparison results, it was found that the R^2 of $PM_{2.5}$ estimated by the DF model was about 0.03–0.06 higher than other models. The DF model can effectively improve the estimated $PM_{2.5}$ accuracy using Himawari-8 AOD data.

There were also significant differences in model performance on the seasonal scale, and the results are shown in Fig. 2 (A–D). The R^2 values were 0.87, 0.9, and 0.88, and RMSE (MAE) values were 11.6 μg/m^3 (7.7 μg/m^3), 11.06 μg/m^3 (7.36 μg/m^3), and 15.42 μg/m^3 (9.21 μg/m^3), in spring, autumn, and winter models, respectively. Due to the small sample size, the model performed poorly in summer, with R^2 = 0.76 (RMSE = 8.6 μg/m^3, MAE = 6.08 μg/m^3). Burning fossil fuels for heating (Xiao et al., 2015) resulted in a higher RMSE in winter than in the other three seasons, and lower RMSE in summer due to reduced emissions and increased precipitation (Witkowska and Lewandowska, 2016). The estimated and measured values of $PM_{2.5}$ were validated on different time scales (Fig. 2, E–H). Daily, monthly, seasonal, and annual R^2 values were 0.9, 0.91, 0.93, and 0.93, RMSE (MAE) values were 10.54 μg/m^3, 6.43 μg/m^3, 4.96 μg/m^3, and 3.55 μg/m^3 (6.63 μg/m^3, 3.77 μg/m^3, 2.96 μg/m^3, and 1.97 μg/m^3), and the fitting slopes were 0.88, 0.89, 0.91, and 0.91, respectively. The results indicated that estimated $PM_{2.5}$ derived from DF can provide reliable data for monitoring the spatial variation and temporal trend of $PM_{2.5}$ pollution in China.

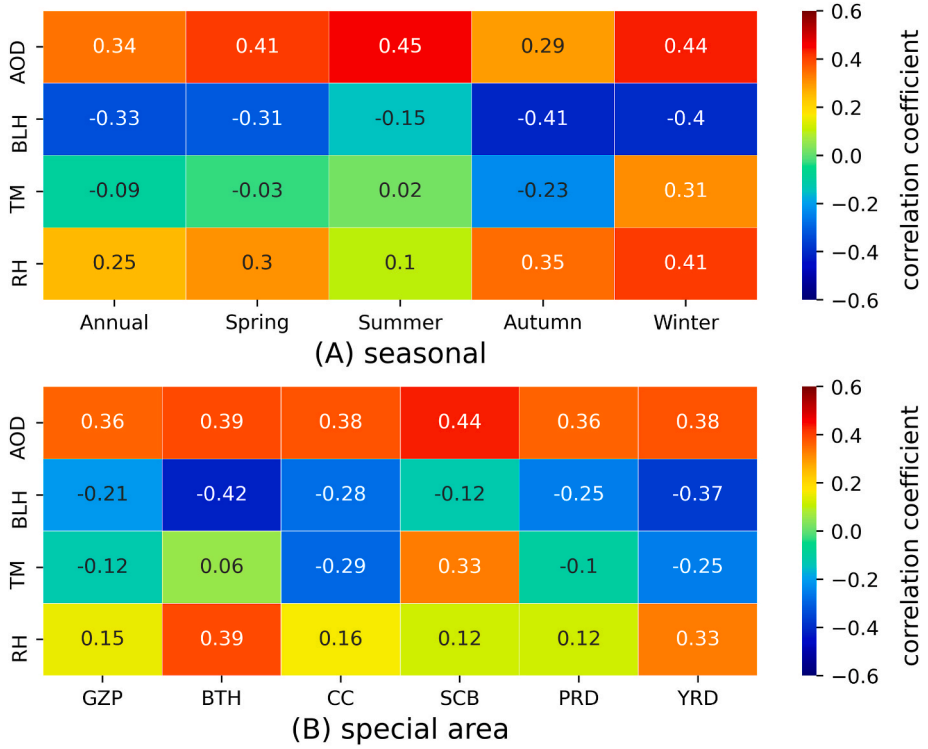

Fig. 4. Correlation between AOD, BLH, TM, and RH and $PM_{2.5}$, (A) different seasons, (B) different areas. The color and number indicate the correlation coefficient. (For interpretation of the references to color in this figure legend, the reader is referred to the Web version of this article.)

3.2. Spatial scale validation results

As shown in Fig. 3, the model performance exhibited spatial differences. The results indicated that R^2 was generally higher, and the RMSE and MAE were lower in the dense station areas. We found that the regions with good model performance were consistent with those regions with high $PM_{2.5}$ values in China, and those regions with poor model performance were primarily distributed in western and northeastern China. This may be related to the better data quality from heavily polluted areas. The statistical results showed that approximately 70%, 75%, and 76% of grid points had $R^2 > 0.6$, RMSE <13 μg/m^3, and MAE <9 μg/m^3, respectively. As shown in Figure S4, in the Beijing–Tianjin–Hebei region, Central China, Yangtze River Delta, and Pearl River Delta, the model performance was excellent, with R^2 was 0.9, 0.91, 0.89, and 0.89, respectively; and R^2 in the Sichuan Basin and Guanzhong Plain was lower, with 0.84 and 0.88, respectively.

3.3. Influence of important features on model performance

Feature importance represents the total gains of splits that use the feature during model construction (Liu et al., 2021; Wei et al., 2021). As shown in Figure S5, AOD made the highest contribution to the DF model, with a feature importance of 18%. Several meteorological factors also had significant effects on the model, and the feature importance of BLH, TM, and RH were 16%, 8%, and 6%, respectively. The contributions of factors were analyzed in different regions and seasons (Figure S6). For different seasons, when both the AOD and BLH feature importance scores were higher than 0.1, the model performance is better. However, in summer, the feature importance of AOD is as high as 0.26, but the feature importance of BLH is very low, and the model performance is poor. On the other hand, in addition to AOD and BLH, RH and TM contributions should also be considered for different regions. Therefore, in different seasons and regions, features with higher feature importance are more likely to determine the performance of AOD-$PM_{2.5}$ model. In general, AOD, time, BLH, RH and TM show higher feature importance in regions and seasons with better model performance. As shown in Figure S7, when adding features to the model in descending order of importance values (Figure S7 (A)), R^2 first rose rapidly, reaching about 0.8 when the fifth feature was added, and then grew slowly. Similarly, when adding features to the model in ascending order (Figure S7 (B)), R^2 increased slowly at first, and did not begin to increase rapidly until the sixth feature was added.

To discuss the influence of important features on model performance, we analyzed the correlation between AOD, BLH, TM, RH, and $PM_{2.5}$ in different seasons and regions, and the results are shown in Fig. 4 and Figure S8. The seasonal correlation between AOD and $PM_{2.5}$ was higher in spring, summer, and winter, and lower in autumn. However, the correlation between meteorological factors and $PM_{2.5}$ was higher in autumn and winter, followed by spring, and was lowest in summer. Combined with R^2 and the correlation coefficient, we found that R^2 is related to the correlation between meteorological factors and $PM_{2.5}$; the two values have similar variations. The results indicate that meteorological factors affect the model performance in different seasons. The correlation results between meteorological features and $PM_{2.5}$ in different regions, were similar. For example, the correlation between AOD and $PM_{2.5}$ in Beijing–Tianjin–Hebei and Central China was lower than that in the Sichuan Basin, but the correlation between meteorological factors and $PM_{2.5}$ was higher than that in Sichuan Basin, and the model R^2 values in these two regions were higher than those in the Sichuan Basin. Thus, factors with high feature importance had a significant influence on the model performance, and the correlation between these factors and $PM_{2.5}$ had a substantial impact on the model performance.

To further explore the relationship between model performance and important features, R^2 and RMSE scatter diagrams with important features were drawn, and the results are shown in Figure S9. low R^2 values may occur near the extreme values of AOD and meteorological factor values. When AOD values were large, RMSE had both high and low values. RMSE changed little with the increase of relative humidity. RMSE decreased with the increase of BLH and first increased and then

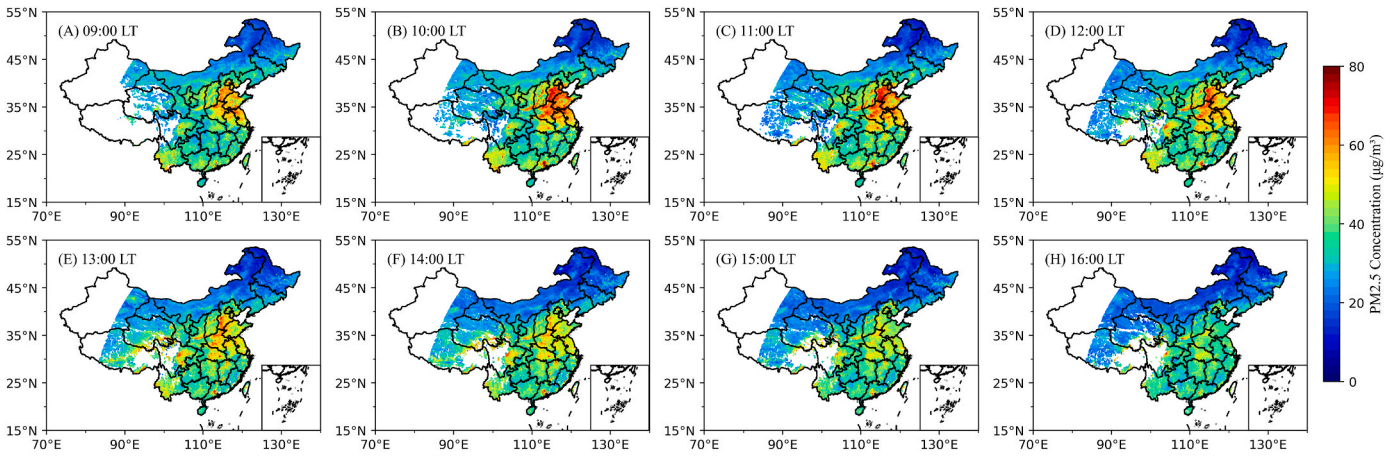

Fig. 5. Diurnal variation in $PM_{2.5}$ concentration in China. A-H represents the $PM_{2.5}$ concentrations between 09:00–16:00 Beijing time.

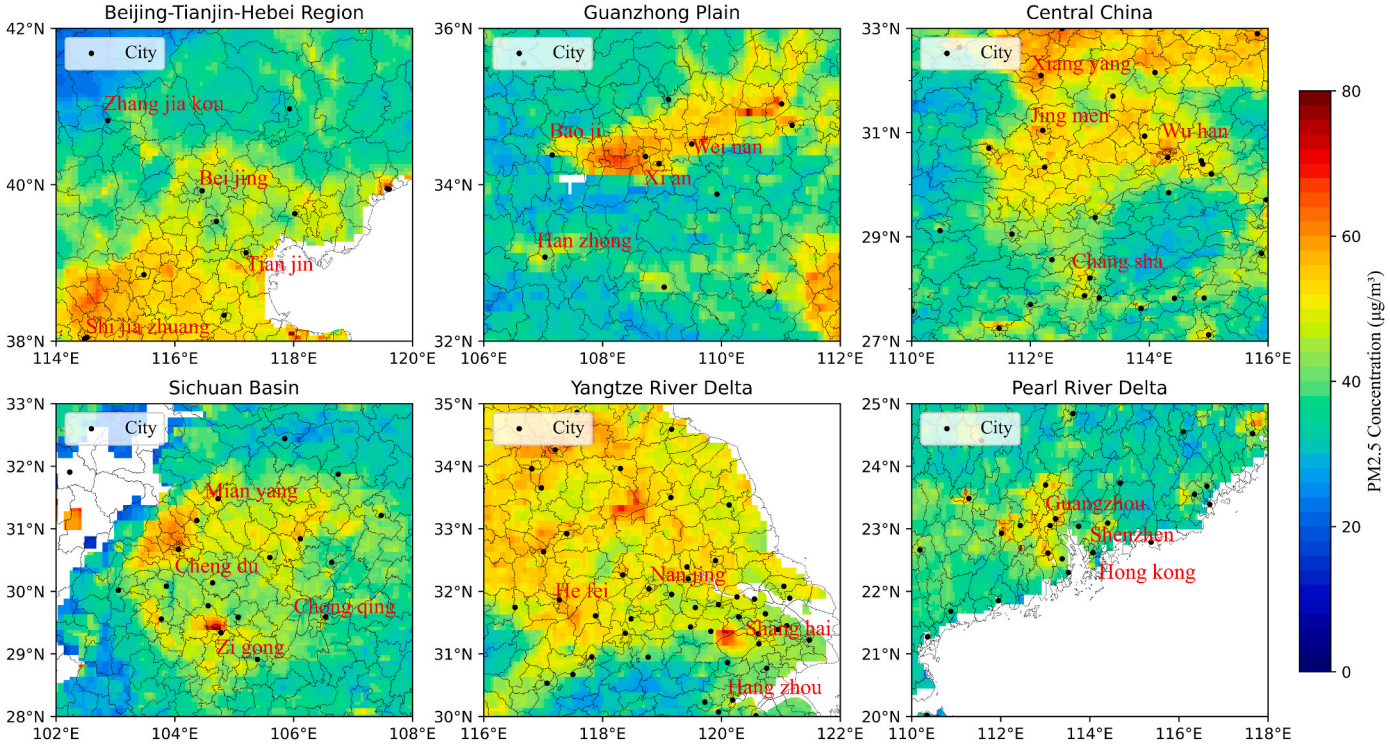

Fig. 6. Distribution of $PM_{2.5}$ concentration in the six urban agglomerations in China. Black dots represent cities, and some big cities are shown in red. Each region name was displayed on the submap title. (For interpretation of the references to color in this figure legend, the reader is referred to the Web version of this article.)

decreased with the increase of TM. The influence of inversion factors on $PM_{2.5}$ can explain these phenomena (Gupta et al., 2006; Li et al., 2016; Han et al., 2018; Lv et al., 2019; Le et al., 2020). These results indicated that the model was affected by the numerical size of the estimated factor.

4. Spatial distribution of $PM_{2.5}$

4.1. Temporal variation in $PM_{2.5}$

Input the hourly independent variables into the model to calculate the hourly $PM_{2.5}$ concentration data. Then calculated the annual average of hourly $PM_{2.5}$ data from 09:00 to 16:00 (Beijing time). Finally, the diurnal variation of $PM_{2.5}$ from 09:00 to 16:00 in 2018 was shown in Fig. 5. The concentration of $PM_{2.5}$ reached its peak (33 μg/m^3) at 10:00–11:00, and then decreased significantly (28 μg/m^3) from 15:00–16:00. There was serious pollution in the Beijing-Tianjin-Hebei region, and the daily concentration range of $PM_{2.5}$ was 34.67 μg/m^3–53.10 μg/m^3, with a maximum of 132.67 μg/m^3. Heavily polluted areas in southern China included the Sichuan Basin and the Pearl River Delta, where $PM_{2.5}$ concentrations exceeded 60 μg/m^3. The pollution was not serious in Inner Mongolia, Qinghai, and northeastern China, and the daily maximum value of $PM_{2.5}$ was less than 40 μg/m^3. Due to the bright surface and cloud cover, effective data could not be obtained from China's Tibetan Plateau.

Figure S10 used the same calculation method, seasonal average value is obtained from the hourly $PM_{2.5}$ data. The average concentration of $PM_{2.5}$ in China was 32.61 μg/m^3, 24.29 μg/m^3, 28.72 μg/m^3, and 42.18 μg/m^3, during spring, summer, autumn, and winter, respectively. The $PM_{2.5}$ concentration distribution indicated that the Beijing–Tianjin–Hebei region, central China, the Yangtze River Delta, and the Sichuan Basin are seriously polluted, particularly in winter. These

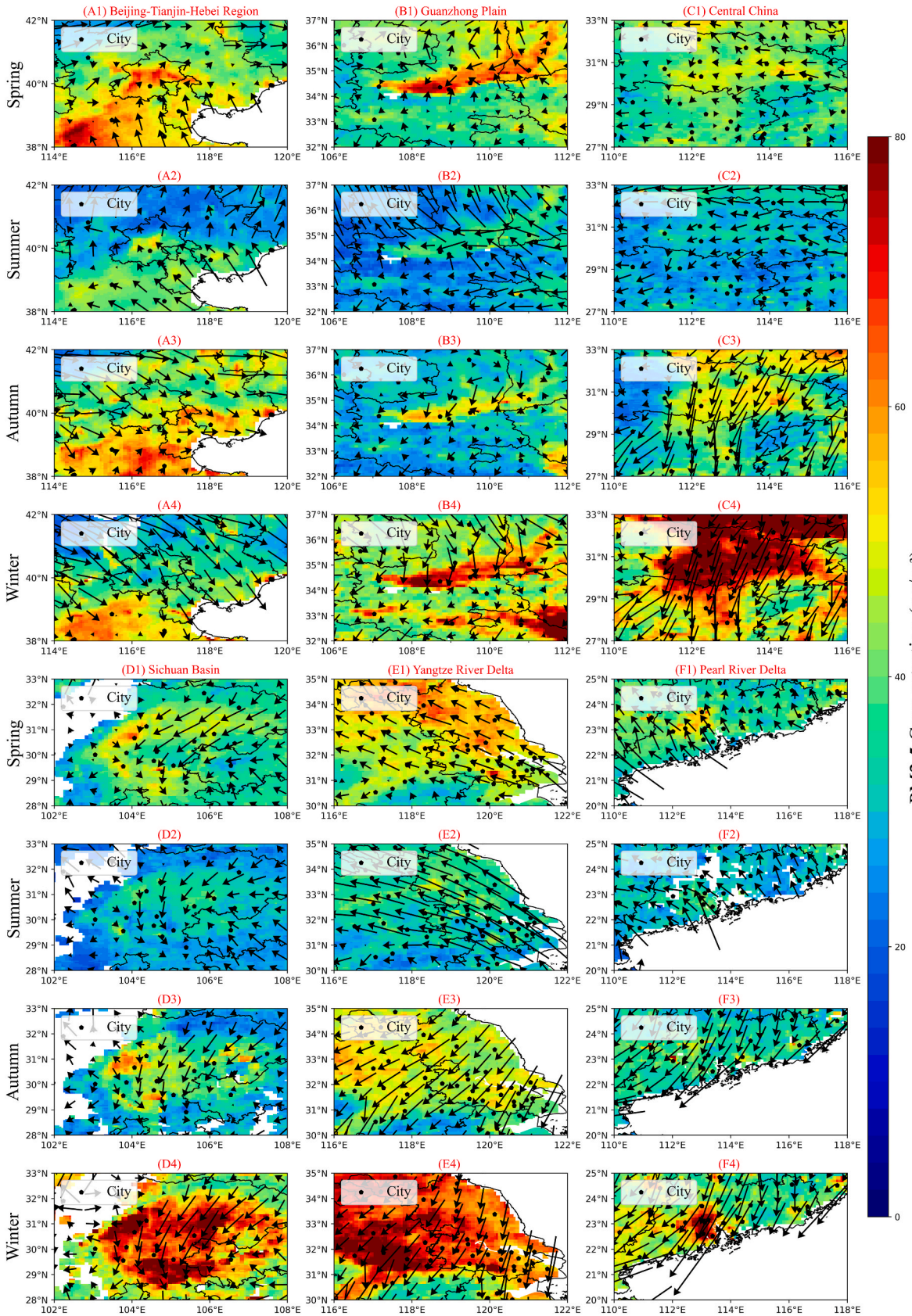

Fig. 7. Distribution of $PM_{2.5}$ and wind field. Black dots represent cities, and arrows represent wind direction. Each region name was displayed on the submap title. A: Beijing-Tianjin-Hebei Region; B: Guanzhong Plain; C: Central China; D: Sichuan Basin; E: Yangtze River Delta; F: Pearl River Delta. Subscripts 1, 2, 3 and 4 represent spring, summer, autumn, and winter, respectively. The length of the arrows represents the wind speed.

areas have a large population and burn a large amount of fossil fuels for heating in winter, resulting in a surge in $PM_{2.5}$ (Zhang et al., 2020b). $PM_{2.5}$ pollution is also very serious in spring, but the area with high $PM_{2.5}$ concentration primarily occurs in North China, which is related to the long-range dust transport caused by spring dust storm weather (Liu et al., 2020b). Due to lower emissions and higher precipitation in summer and autumn, and the elimination of $PM_{2.5}$ in these two seasons, $PM_{2.5}$ pollution is low (Yan et al., 2018).

4.2. Distribution of city-level $PM_{2.5}$

The study used AOD with a resolution of 5 km to estimate $PM_{2.5}$, which can reflect the concentration distribution of $PM_{2.5}$ on an urban spatial scale. Fig. 6 shows the average $PM_{2.5}$ concentrations in six urban agglomerations in China. The results indicate that $PM_{2.5}$ pollution was severe near some cities, such as Xi 'an, Chengdu, and Wuhan, where the annual average $PM_{2.5}$ concentration reached 60 μg/m^3. The $PM_{2.5}$ concentration in Beijing, Guangzhou, and Shenzhen was approximately 40 μg/m^3. Shanghai, China's economic center, was not seriously polluted, with an average annual $PM_{2.5}$ of less than 40 μg/m^3. Generally, $PM_{2.5}$ estimated by the Himawari-8 AOD and DF model can reflect the pollution status of county-level administrative units in China, and is relatively consistent with large local emission sources (Li et al., 2017a; Liu et al., 2020a).

4.3. Relationship between $PM_{2.5}$ distribution and wind field

The wind field is conducive for pollutant diffusion (Wu et al., 2021). Fig. 7 shows the seasonal distribution of $PM_{2.5}$ and wind field in the six urban agglomerations. The results indicate that the pollutant diffusion direction was consistent with the wind field direction. The pollutants in the Guanzhong Plain diffused from east to west along the wind direction and accumulated at approximately 34° N and 108° E, forming a highly polluted area. In spring and summer, southeast winds prevailed in the Beijing–Tianjin–Hebei region, and the barrier formed by the Yanshan Mountains created a $PM_{2.5}$ high-value area in northwestern Beijing. However, in autumn and winter, the prevailing wind in the region was northwesterly, and the pollutants transferred to the southeast. Moreover, the wind speed was higher in winter, and the $PM_{2.5}$ concentration was lower than that in autumn. In winter, the north wind induced the pollutants in the central region to spread to the south, causing serious pollution. In autumn, pollutants also moved southward, but the pollution was not severe. In spring and summer, the $PM_{2.5}$ concentration was low, and the pollutants moved westward with the wind field. The annual wind field in the northern Sichuan Basin was from the northeast, blocked by mountains, and turned to the northwest. The pollutants at the basin edge were distributed along the wind direction, and some pollutants were transported to the center of the basin. The diffusion of pollutants in the Yangtze River Delta was also obvious. Southeast wind prevailed in spring and summer, and the pollutants diffused to the northwest, while northeast winds prevailed in autumn and winter, and the pollutants diffused to the southwest. Blocked by mountains, serious pollution occurred near 32° N and 117° E in winter. The pollutants in the Pearl River Delta were concentrated in Guangzhou, and the pollutants spread to the northwest and southwest in spring and winter, respectively. These results indicate that $PM_{2.5}$ derived from the Himawari-8 AOD and DF model can reflect the pollution conditions well. The coordination of the wind field and terrain can also indicate the diffusion direction of pollutants, which can provide a scientific basis for local pollution control.

5. Conclusions

Understanding the temporal and spatial distribution of $PM_{2.5}$ is of great significance for pollution control. This study used a DF model, combined with Himawari-8 AOD, meteorological factors, and geographic information to estimate $PM_{2.5}$ in China in 2018. The main results indicate the following:

(1) The DF model can effectively capture the hourly $PM_{2.5}$ concentration near the ground, with a sample-based cross-validation R^2 range of 0.82–0.91. The estimated $PM_{2.5}$ was consistent with the observed $PM_{2.5}$, with RMSE ranging from 8.79 μg/m^3–14.72 μg/m^3. The R^2 of $PM_{2.5}$ estimated by the DF model was about 0.03–0.06 higher than other models.
(2) Factors with high feature importance had a significant influence on the model performance. Correlation analysis indicated that model performance was related to the correlation between the estimated factors and $PM_{2.5}$. The model R^2 varied significantly with each factor value, but the model performance is typically poor under extreme meteorological conditions.
(3) $PM_{2.5}$ concentration shows obvious diurnal variation, which peaked (33 μg/m^3) at 10:00–11:00, and then dropped to 28 μg/m^3 at 15:00–16:00. The model can also capture the urban-scale $PM_{2.5}$ concentration distribution, and the pollutants are primarily distributed near cities.

There were some pollutant accumulation areas in China affected by terrain and wind, which should be prioritized when formulating pollution prevention and control measures. In the future, we could combine the estimation of vertical $PM_{2.5}$ (Chen et al., 2021) with this study to construct the three-dimensional distribution of $PM_{2.5}$, which will be more conducive to understand the evolution of pollutants.

Credit author statement

Bin Chen: Conceptualization, Methodology, Writing- Reviewing and Editing. Zhihao Song: Conceptualization, Software, Methodology, Data curation, Writing – original draft. Jianping Huang: Supervision, Project administration and Editing.

Declaration of competing interest

The authors declare that they have no known competing financial interests or personal relationships that could have appeared to influence the work reported in this paper.

Acknowledgements

The work Supported by the National Key Research and Development Program of China (Grant number 2019YFA0606800) and the National Natural Science Foundation of China (Grant 41775021). The $PM_{2.5}$ data were obtained from https://www.aqistudy.cn/historydata/. The Himawari-8 AOD data provided by the Japan Meteorological Agency, download from: http://www.eorc.jaxa.jp/ptree/index.html. And the ERA-5 data are available from https://cds.climate.copernicus.eu/cdsapp#!/dataset/reanalysis-era5-land?tab=overview. The authors would like to thank China National Environmental Monitoring Center and European Centre for Medium-Range Weather Forecasts for their datasets.

Appendix A. Supplementary data

Supplementary data to this article can be found online at https://doi.org/10.1016/j.envpol.2022.118826.

References

Andersson, A., Deng, J., Du, K., Zheng, M., Yan, C., Sköld, M., Gustafsson, Ö., 2015. Regionally-varying combustion sources of the january 2013 severe haze events over eastern China. Environ. Sci. Technol. 49, 2038–2043.

Budnik, L.T., Casteleyn, L., Paschalidou, A.K., Kassomenos, P., 2019. Pollution in living and working environments, climate variability, and their impact on non-communicable disease burden. Science of the Total Environment,660 593–594.
Chen, B., Song, Z., Pan, F., Huang, Y., 2021. Obtaining vertical distribution of PM2.5 from CALIOP data and machine learning algorithms. Sci. Total Environ. 805, 150338.
Chen, B., Song, Z., Shi, B., Li, M., 2022. An interpretable deep forest model for estimating hourly PM10 concentration in China using Himawari-8 data. Atmos. Environ. (268), 118827.
Chen, J., Yin, J., Zang, L., Zhang, T., Zhao, M., 2019. Stacking machine learning model for estimating hourly PM2.5 in China based on Himawari 8 aerosol optical depth data. Science of the Total Environment,697 134021.
Chen, M., Guo, S., Hu, M., Zhang, X., 2020. The spatiotemporal evolution of population exposure to PM2.5 within the Beijing-Tianjin-Hebei urban agglomeration, China. J. Clean. Prod. 265, 121708.
Chen, W.-R., Singh, A., Pani, S.K., Chang, S.-Y., Chou, C.C.K., Chang, S.-C., Chuang, M.-T., Lin, N.-H., Huang, C.-H., Lee, C.-T., 2021c. Real-time measurements of PM2.5 water-soluble inorganic ions at a high-altitude mountain site in the western North Pacific: impact of upslope wind and long-range transported biomass-burning smoke. Atmospheric Research,260 105686.
Cheng, Z., Wang, S., Jiang, J., Fu, Q., Chen, C., Xu, B., Yu, J., Fu, X., Hao, J., 2013. Long-term trend of haze pollution and impact of particulate matter in the Yangtze River Delta, China. Environmental Pollution,182 101–110.
China Environmental Science Press, 2012. Ambient air quality standards. GB, 3095–2012. (Available online.
Chu, D.A., Kaufman, Y.J., Ichoku, C., Remer, L.A., Tanré, D., Holben, B.N., 2002. Validation of MODIS aerosol optical depth retrieval over land. Geophys. Res. Lett. 29. MOD2-1-MOD2-4.
Cohen, A.J., Brauer, M., Burnett, R., Anderson, H.R., Frostad, J., Estep, K., Balakrishnan, K., Brunekreef, B., Dandona, L., Dandona, R., Feigin, V., Freedman, G., Hubbell, B., Jobling, A., Kan, H., Knibbs, L., Liu, Y., Martin, R., Morawska, L., Pope, C.A., Shin, H., Straif, K., Shaddick, G., Thomas, M., van Dingenen, R., van Donkelaar, A., Vos, T., Murray, C.J.L., Forouzanfar, M.H., 2017. Estimates and 25-year trends of the global burden of disease attributable to ambient air pollution: an analysis of data from the Global Burden of Diseases Study 2015. The Lancet,389 1907–1918.
Dimitriou, K., Paschalidou, A.K., Kassomenos, P.A., 2013. Assessing air quality with regards to its effect on human health in the European Union through air quality indices. Ecol. Indicat. 27, 108–115.
Duvall, R.M., Norris, G.A., Burke, J.M., Olson, D.A., Vedantham, R., Williams, R., 2012. Determining spatial variability in PM2.5 source impacts across Detroit, MI. Atmos. Environ. 47, 491–498.
Fu, Q., Zhuang, G., Wang, J., Xu, C., Huang, K., Li, J., Hou, B., Lu, T., Streets, D.G., 2008. Mechanism of formation of the heaviest pollution episode ever recorded in the Yangtze River Delta, China. Atmos. Environ. 42, 2023–2036.
Gao, L., Chen, L., Li, C., Li, J., Che, H., Zhang, Y., 2021. Evaluation and possible uncertainty source analysis of JAXA Himawari-8 aerosol optical depth product over China. Atmospheric Research,248 105248.
Gao, M., Carmichael, G.R., Wang, Y., Saide, P.E., Yu, M., Xin, J., Liu, Z., Wang, Z., 2016. Modeling study of the 2010 regional haze event in the North China Plain. Atmos. Chem. Phys. 16, 1673–1691.
Ge, B., Yang, L., Chen, X., Mei, X., Liu, L., 2018. Study on aerosol optical depth retrieval over land from Himawari-8 data based on dark target method. Journal of Remote Sensing 22, 38–50.
Guarnieri, M., Balmes, J.R., 2014. Outdoor air pollution and asthma. The Lancet,383 1581–1592.
Guo, J.-P., Zhang, X.-Y., Che, H.-Z., Gong, S.-L., An, X., Cao, C.-X., Guang, J., Zhang, H., Wang, Y.-Q., Zhang, X.-C., Xue, M., Li, X.-W., 2009. Correlation between PM concentrations and aerosol optical depth in eastern China. Atmos. Environ. 43, 5876–5886.
Guo, J., Xia, F., Zhang, Y., Liu, H., Li, J., Lou, M., He, J., Yan, Y., Wang, F., Min, M., Zhai, P., 2017. Impact of diurnal variability and meteorological factors on the PM2.5-AOD relationship: implications for PM2.5 remote sensing. Environmental Pollution,221 94–104.
Gupta, P., Christopher, S.A., Wang, J., Gehrig, R., Lee, Y., Kumar, N., 2006. Satellite remote sensing of particulate matter and air quality assessment over global cities. Atmos. Environ. 40, 5880–5892.
Han, S., Liu, J., Hao, T., Zhang, Y., Li, P., Yang, J., Wang, Q., Cai, Z., Yao, Q., Zhang, M., Wang, X., 2018. Boundary layer structure and scavenging effect during a typical winter haze-fog episode in a core city of BTH region, China. Atmospheric Environment,179 187–200.
Hu, X., Waller, L.A., Lyapustin, A., Wang, Y., Al-Hamdan, M.Z., Crosson, W.L., Estes, M. G., Estes, S.M., Quattrochi, D.A., Puttaswamy, S.J., Liu, Y., 2014. Estimating ground-level PM2.5 concentrations in the Southeastern United States using MAIAC AOD retrievals and a two-stage model. Rem. Sens. Environ. 140, 220–232.
Huang, D., Xu, J., Zhang, S., 2012a. Valuing the health risks of particulate air pollution in the Pearl River Delta, China. Environ. Sci. Pol. 15, 38–47.
Huang, K., Zhuang, G., Lin, Y., Fu, J.S., Wang, Q., Liu, T., Zhang, R., Jiang, Y., Deng, C., Fu, Q., Hsu, N.C., Cao, B., 2012b. Typical types and formation mechanisms of haze in an Eastern Asia megacity. Shanghai. Atmos. Chem. Phys. 12, 105–124.
Ji, D., Wang, Y., Wang, L., Chen, L., Hu, B., Tang, G., Xin, J., Song, T., Wen, T., Sun, Y., Pan, Y., Liu, Z., 2012. Analysis of heavy pollution episodes in selected cities of northern China. Atmos. Environ. 50, 338–348.
Kassomenos, P.A., Vardoulakis, S., Chaloulakou, A., Paschalidou, A.K., Grivas, G., Borge, R., Lumbreras, J., 2014. Study of PM10 and PM2.5 levels in three European cities: analysis of intra and inter urban variations. Atmos. Environ. 87, 153–163.
Le, T., Wang, Y., Liu, L., Yang, J., Yung Yuk, L., Li, G., Seinfeld John, H., 2020. Unexpected air pollution with marked emission reductions during the COVID-19 outbreak in China. Science 369, 702–706.
Li, H., Shahbaz, M., Jiang, H., Dong, K., 2021. Is natural gas consumption mitigating air pollution? Fresh evidence from national and regional analysis in China. Sustain. Prod. Consum. 27, 325–336.
Li, M., Liu, H., Geng, G., Hong, C., Liu, F., Song, Y., Tong, D., Zheng, B., Cui, H., Man, H., Zhang, Q., He, K., 2017a. Anthropogenic emission inventories in China: a review. Natl. Sci. Rev. 4, 834–866.
Li, T., Shen, H., Yuan, Q., Zhang, X., Zhang, L., 2017b. Estimating ground-level PM2.5 by fusing satellite and station observations: a geo-intelligent deep learning approach. Geophys. Res. Lett. 44, 11,985-911,993.
Li, Z., Zhang, Y., Shao, J., Li, B., Hong, J., Liu, D., Li, D., Wei, P., Li, W., Li, L., Zhang, F., Guo, J., Deng, Q., Wang, B., Cui, C., Zhang, W., Wang, Z., Lv, Y., Xu, H., Chen, X., Li, L., Qie, L., 2016. Remote sensing of atmospheric particulate mass of dry PM2.5 near the ground: method validation using ground-based measurements. Rem. Sens. Environ. 173, 59–68.
Liu, F., Tan, Q., Jiang, X., Yang, F., Jiang, W., 2019a. Effects of relative humidity and PM2.5 chemical compositions on visibility impairment in Chengdu, China. J. Environ. Sci. 86, 15–23.
Liu, J., Han, Y., Tang, X., Zhu, J., Zhu, T., 2016. Estimating adult mortality attributable to PM2.5 exposure in China with assimilated PM2.5 concentrations based on a ground monitoring network. Sci. Total Environ. 568, 1253–1262.
Liu, J., Zheng, Y., Geng, G., Hong, C., Li, M., Li, X., Liu, F., Tong, D., Wu, R., Zheng, B., He, K., Zhang, Q., 2020a. Decadal changes in anthropogenic source contribution of PM2.5 pollution and related health impacts in China, 1990–2015. Atmos. Chem. Phys. 20, 7783–7799.
Liu, L., Duan, Y., Li, L., Xu, L., Yang, Y., Cu, X., 2020b. Spatiotemporal trends of PM2.5 concentrations and typical regional pollutant transport during 2015–2018 in China. Urban Clim. 34, 100710.
Liu, Q., Wang, S., Zhang, W., Li, J., Dong, G., 2019b. The effect of natural and anthropogenic factors on PM2.5: empirical evidence from Chinese cities with different income levels. Sci. Total Environ. 653, 157–167.
Liu, Z., Qi, Z., Ni, X., Dong, M., Ma, M., Xue, W., Zhang, Q., Wang, J., 2021. How to apply O3 and PM2.5 collaborative control to practical management in China: a study based on meta-analysis and machine learning. Sci. Total Environ. 772, 145392.
Lv, D., Chen, Y., Zhu, T., Li, T., Shen, F., Li, X., Mehmood, T., 2019. The pollution characteristics of PM10 and PM2.5 during summer and winter in Beijing, Suning and Islamabad. Atmos. Pollut. Res. 10, 1159–1164.
Ma, S., Shao, M., Zhang, Y., Dai, Q., Xie, M., 2021. Sensitivity of PM2.5 and O3 pollution episodes to meteorological factors over the North China Plain. Sci. Total Environ. 792, 148474.
Ma, X., Wang, J., Yu, F., Jia, H., Hu, Y., 2016. Can MODIS AOD be employed to derive PM2.5 in Beijing-Tianjin-Hebei over China? Atmos. Res. 181, 250–256.
Ma, Z., Hu, X., Huang, L., Bi, J., Liu, Y., 2014. Estimating ground-level PM2.5 in China using satellite remote sensing. Environ. Sci. Technol. 48, 7436–7444.
Pan, L., Xu, J., Tie, X., Mao, X., Gao, W., Chang, L., 2019. Long-term measurements of planetary boundary layer height and interactions with PM2.5 in Shanghai, China. Atmos. Pollut. Res. 10, 989–996.
Pinto, J.P., Lefohn, A.S., Shadwick, D.S., 2004. Spatial variability of PM2.5 in urban areas in the United States. J. Air Waste Manag. Assoc. 54, 440–449.
Qin, K., Zou, J., Guo, J., Lu, M., Bilal, M., Zhang, K., Ma, F., Zhang, Y., 2018. Estimating PM1 concentrations from MODIS over Yangtze River Delta of China during 2014–2017. Atmos. Environ. 195, 149–158.
Rodriguez, J.D., Perez, A., Lozano, J.A., 2010. Sensitivity analysis of k-fold cross validation in prediction error estimation. IEEE Trans. Pattern Anal. Mach. Intell. 32, 569–575.
Shen, H., Li, T., 2019. Progress of remote sensing mapping of atmospheric PM2.5. Acta Geod. Cartogr. Sinica 48.
Song, Z., Chen, B., Huang, Y., Dong, L., Yang, T., 2021. Estimation of PM2.5 concentration in China using linear hybrid machine learning model. Atmos. Meas. Tech. 14, 5333–5347.
Stafoggia, M., Bellander, T., Bucci, S., Davoli, M., de Hoogh, K., de' Donato, F., Gariazzo, C., Lyapustin, A., Michelozzi, P., Renzi, M., Scortichini, M., Shtein, A., Viegi, G., Kloog, I., Schwartz, J, 2019. Estimation of daily PM10 and PM2.5 concentrations in Italy, 2013–2015, using a spatiotemporal land-use random-forest model. Environ. Int. 124, 170–179.
Sun, L., Wei, J., Duan, D.H., Guo, Y.M., Yang, D.X., Jia, C., Mi, X.T., 2016. Impact of Land-Use and Land-Cover Change on urban air quality in representative cities of China. J. Atmos. Sol. Terr. Phys. 142, 43–54.
Ul-Saufie, A.Z., Yahaya, A.S., Ramli, N.A., Rosaida, N., Hamid, H.A., 2013. Future daily PM10 concentrations prediction by combining regression models and feedforward backpropagation models with principle component analysis (PCA). Atmos. Environ. 77, 621–630.
Wang, X., Sun, W., 2019. Meteorological parameters and gaseous pollutant concentrations as predictors of daily continuous PM2.5 concentrations using deep neural network in Beijing–Tianjin–Hebei, China. Atmos. Environ. 211, 128–137.
Wei, J., Huang, W., Li, Z., Xue, W., Peng, Y., Sun, L., Cribb, M., 2019. Estimating 1-km-resolution PM2.5 concentrations across China using the space-time random forest approach. Rem. Sens. Environ. 231, 111221.
Wei, J., Li, Z., Pinker, R.T., Wang, J., Sun, L., Xue, W., Li, R., Cribb, M., 2021. Himawari-8-derived diurnal variations in ground-level PM2.5 pollution across China using the fast space-time Light Gradient Boosting Machine (LightGBM). Atmos. Chem. Phys. 21, 7863–7880.

Witkowska, A., Lewandowska, A.U., 2016. Water soluble organic carbon in aerosols (PM1, PM2.5, PM10) and various precipitation forms (rain, snow, mixed) over the southern Baltic Sea station. Sci. Total Environ. 573, 337–346.
Wu, J., Luo, K., Wang, Y., Wang, Z., 2021. Urban road greenbelt configuration: the perspective of PM2.5 removal and air quality regulation. Environ. Int. 157, 106786.
Wu, Y., Zhang, F., Wu, K., Min, M., Li, W., Liu, R., 2020. Best water vapor information layer of himawari-8-based water vapor bands over east Asia. Sensors 20.
Xiao, Q., Ma, Z., Li, S., Liu, Y., 2015. The impact of winter heating on air pollution in China. PLoS One e0117311.
Xiao, Q., Wang, Y., Chang, H.H., Meng, X., Geng, G., Lyapustin, A., Liu, Y., 2017. Full-coverage high-resolution daily PM2.5 estimation using MAIAC AOD in the Yangtze River Delta of China. Rem. Sens. Environ. 199, 437–446.
Xiao, Z.-m., Zhang, Y.-f., Hong, S.-m., Bi, X.-h., Jiao, L., Feng, Y.-c., Wang, Y.-q., 2011. Estimation of the main factors influencing haze, based on a long-term monitoring campaign in hangzhou, China. Aerosol Air Qual. Res. 11, 873–882.
Xiong, H.-B., Chen, J., Ma, X., Fang, M.-Y., 2021. Estimating the PM2.5 concentration over anhui province, China, using the himawari-8 AOD and a GAM/BME model. Atmos. Pollut. Res. 12, 101110.
Xu, P., Chen, Y., Ye, X., 2013. Haze, air pollution, and health in China. Lancet 382, 2067.
Xu, Q., Chen, X., Yang, S., Tang, L., Dong, J., 2021. Spatiotemporal relationship between Himawari-8 hourly columnar aerosol optical depth (AOD) and ground-level PM2.5 mass concentration in mainland China. Sci. Total Environ. 765, 144241.
Yan, D., Lei, Y., Shi, Y., Zhu, Q., Li, L., Zhang, Z., 2018. Evolution of the spatiotemporal pattern of PM2.5 concentrations in China – a case study from the Beijing-Tianjin-Hebei region. Atmos. Environ. 183, 225–233.
Yan, X., Zang, Z., Jiang, Y., Shi, W., Guo, Y., Li, D., Zhao, C., Husi, L., 2021. A Spatial-Temporal Interpretable Deep Learning Model for improving interpretability and predictive accuracy of satellite-based PM2.5. Environ. Pollut. 273, 116459.
Yang, Q., Yuan, Q., Yue, L., Li, T., Shen, H., Zhang, L., 2019. The relationships between PM2.5 and aerosol optical depth (AOD) in mainland China: about and behind the spatio-temporal variations. Environ. Pollut. 248, 526–535.
Yang, X., Zhao, C., Luo, N., Zhao, W., Shi, W., Yan, X., 2020. Evaluation and Comparison of Himawari-8 L2 V1.0, V2.1 and MODIS C6.1 aerosol products over Asia and the oceania regions. Atmos. Environ. 220, 117068.
Yoshida, M., Kikuchi, M., Nagao, T.M., Murakami, H., Nomaki, T., Higurashi, A., 2018. Common retrieval of aerosol properties for imaging satellite sensors. Journal of the Meteorological Society of Japan. Ser. II 96B, 193–209.
Zang, L., Mao, F., Guo, J., Wang, W., Pan, Z., Shen, H., Zhu, B., Wang, Z., 2019. Estimation of spatiotemporal PM1.0 distributions in China by combining PM2.5 observations with satellite aerosol optical depth. Sci. Total Environ. 658, 1256–1264.
Zeng, Z., Gui, K., Wang, Z., Luo, M., Geng, H., Ge, E., An, J., Song, X., Ning, G., Zhai, S., Liu, H., 2021. Estimating hourly surface PM2.5 concentrations across China from high-density meteorological observations by machine learning. Atmospheric Research,254 105516.
Zhang, L., Wilson, J.P., MacDonald, B., Zhang, W., Yu, T., 2020a. The changing PM2.5 dynamics of global megacities based on long-term remotely sensed observations. Environ. Int. 142, 105862.
Zhang, Q., Jiang, X., Tong, D., Davis, S.J., Zhao, H., Geng, G., Feng, T., Zheng, B., Lu, Z., Streets, D.G., Ni, R., Brauer, M., van Donkelaar, A., Martin, R.V., Huo, H., Liu, Z., Pan, D., Kan, H., Yan, Y., Lin, J., He, K., Guan, D., 2017. Transboundary health impacts of transported global air pollution and international trade. Nature 543, 705–709.
Zhang, Q., Zheng, Y., Tong, D., Shao, M., Wang, S., Zhang, Y., Xu, X., Wang, J., He, H., Liu, W., Ding, Y., Lei, Y., Li, J., Wang, Z., Zhang, X., Wang, Y., Cheng, J., Liu, Y., Shi, Q., Yan, L., Geng, G., Hong, C., Li, M., Liu, F., Zheng, B., Cao, J., Ding, A., Gao, J., Fu, Q., Huo, J., Liu, B., Liu, Z., Yang, F., He, K., Hao, J., 2019a. Drivers of improved $PM_{2.5}$ air quality in China from 2013 to 2017. Proc. Natl. Acad. Sci. Unit. States Am. 116, 24463.
Zhang, T., Zang, L., Wan, Y., Wang, W., Zhang, Y., 2019b. Ground-level PM2.5 estimation over urban agglomerations in China with high spatiotemporal resolution based on Himawari-8. Sci. Total Environ. 676, 535–544.
Zhang, W., Liu, B., Zhang, Y., Li, Y., Sun, X., Gu, Y., Dai, C., Li, N., Song, C., Dai, Q., Han, Y., Feng, Y., 2020b. A refined source apportionment study of atmospheric PM2.5 during winter heating period in Shijiazhuang, China, using a receptor model coupled with a source-oriented model. Atmos. Environ. 222, 117157.
Zhang, Y., Li, Z., Bai, K., Wei, Y., Xie, Y., Zhang, Y., Ou, Y., Cohen, J., Zhang, Y., Peng, Z., Zhang, X., Chen, C., Hong, J., Xu, H., Guang, J., Lv, Y., Li, K., Li, D., 2021. Satellite remote sensing of atmospheric particulate matter mass concentration: advances, challenges, and perspectives. Fundamental Research 1, 240–258.
Zhao, X.J., Zhao, P.S., Xu, J., Meng, W., Pu, W.W., Dong, F., He, D., Shi, Q.F., 2013. Analysis of a winter regional haze event and its formation mechanism in the North China Plain. Atmos. Chem. Phys. 13, 5685–5696.
Zhou, Z.-H., Feng, J., 2017. Deep forest: towards an alternative to deep neural networks. CoRR https://doi.org/abs/1702.08835.